

# Computer-automated tuning of semiconductor double quantum dots into the single-electron regime

T. A. Baart,<sup>1,2</sup> P. T. Eendebak,<sup>1,3</sup> C. Reichl,<sup>4</sup> W. Wegscheider,<sup>4</sup> and L. M. K. Vandersypen<sup>1,2</sup>

<sup>1</sup>*QuTech, Delft University of Technology, P.O. Box 5046, 2600 GA Delft, The Netherlands*

<sup>2</sup>*Kavli Institute of Nanoscience, Delft University of Technology, P.O. Box 5046, 2600 GA Delft, The Netherlands*

<sup>3</sup>*Netherlands Organisation for Applied Scientific Research (TNO), P.O. Box 155, 2600 AD Delft, The Netherlands*

<sup>4</sup>*Solid State Physics Laboratory, ETH Zürich, 8093 Zürich, Switzerland*

(Received 30 December 2015; accepted 14 May 2016; published online 24 May 2016)

We report the computer-automated tuning of gate-defined semiconductor double quantum dots in GaAs heterostructures. We benchmark the algorithm by creating three double quantum dots inside a linear array of four quantum dots. The algorithm sets the correct gate voltages for all the gates to tune the double quantum dots into the single-electron regime. The algorithm only requires (1) prior knowledge of the gate design and (2) the pinch-off value of the single gate  $T$  that is shared by all the quantum dots. This work significantly alleviates the user effort required to tune multiple quantum dot devices. *Published by AIP Publishing.* [<http://dx.doi.org/10.1063/1.4952624>]

Electrostatically defined semiconductor quantum dots have been the focus of intense research for the application of solid-state quantum computing.<sup>1–3</sup> In this architecture, quantum bits (qubits) can be defined by the spin state of an electron. Recently, several experiments have shown coherent manipulation of such spins for the purpose of spin-based quantum computation.<sup>4–10</sup> Enabled by advances in device technology, the number of quantum dots that can be accessed is quickly increasing from very few to many.<sup>11,12</sup> Up to date, all these quantum dots have been tuned by “hand.” This is a slow process whereby gate voltages are tweaked carefully, first to reach a regime with one electron in each of the dots and then to adjust the strength of all the tunnel barriers. Defects and variations in the local composition of the heterostructure lead to a disordered background potential landscape, which must be compensated for by the gate voltages. On top, cross-capacitances of each gate to neighboring dots increases the tuning complexity as the number of dots increases. The ability to tune these dots automated by computer algorithms, including tuning of many dots in parallel, is an important ingredient towards the scalability of this approach to create a large-scale quantum computer.

In this letter, we demonstrate the computer automated tuning of double quantum dot (DQD) devices. We have created an algorithm that only requires as input: (1) prior knowledge of the gate design, which is reasonable for future large-scale quantum dot circuits, and (2) the measured pinch-off value of a single gate shared by all the quantum dots. We describe the algorithm used and verify its robustness by creating three independent DQDs inside a quadruple dot array. The algorithm finds the correct gate voltages to tune all DQDs into the single-electron regime, and the computer recognizes that this goal has been achieved.

A scanning electron microscopy (SEM) image of a device nominally identical to the one used is shown in Fig. 1(a). The gate electrodes fabricated on the surface of a GaAs/AlGaAs heterostructure are biased with appropriate voltages to selectively deplete regions of the two-dimensional electron

gas (2DEG) 90 nm below the surface and define the quantum dots. The main function of each gate is as follows: gates  $L$  and  $R$  set the tunnel coupling with the left and right reservoirs, respectively.  $D1$ – $D3$  control the three inter-dot tunnel couplings, and  $P1$ – $P4$  are used to set the electron number in each dot. However, each gate influences the other parameters as well. Changing  $L$ , for example, will also change the electron number in dot 1 and influence the inter-dot tunnel barrier between dots 1 and 2. This needs to be taken into account by the algorithm. Two other nearby quantum dots on top of the qubit array, sensing dots 1 and 2 (SD1 and SD2), are created in a similar way and function as a capacitively coupled charge sensor of the dot array. When positioned on the flank of a Coulomb peak, the conductance through the sensing dot is very sensitive to the number of charges in each of the dots in the array. The changes in conductance are measured using radiofrequency (RF) reflectometry.<sup>13</sup> The high-frequency lines are connected via bias-tees to gates  $P1$ ,  $P3$ , and  $P4$ . The device was cooled inside a dilution refrigerator to a base temperature of  $\sim 15$  mK. All measurements were taken at zero magnetic field.

Before running the algorithm, the user is required to input a range of  $T$ -values for which the algorithm should try to find DQDs. This range is currently determined by measuring the pinch-off value of  $T$  manually, and then choosing a set of gate voltages more negative than this pinch-off value. This step could be automated in future work.

The algorithm consists of 3 steps: (1) to determine the starting values for the gate voltages, we first measure the pinch-off characteristic between each individual gate and the shared  $T$ -gate. Based on those results, we (2) create single quantum dots. The required tunnel barriers acquired in (2) can be used as a starting point to (3) create double dots into the single-electron regime. Subsequently, steps (1) and (2) are used to create the SDs.

To measure the pinch-off characteristic, we apply a small voltage-bias ( $\sim 500$   $\mu$ V) to O4 and measure the current  $I_{\text{array}}$  through the quadruple dot array. Variations in the local

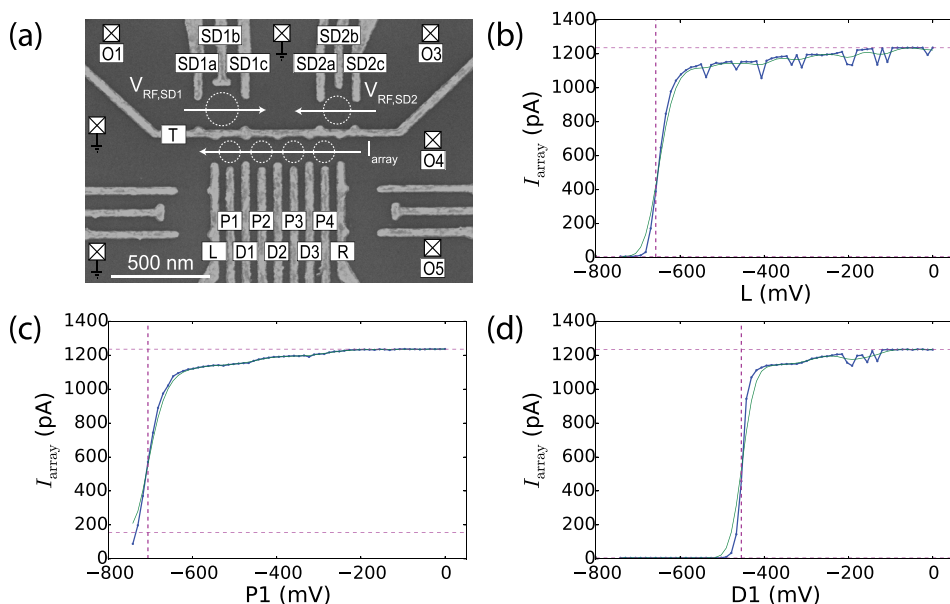


FIG. 1. (a) SEM image of a sample nominally identical to the one used for the measurements. Dotted circles indicate quantum dots, squares indicate Fermi reservoirs in the 2DEG, which are connected to ohmic contacts. O5 is always open during the measurements. The gates that are not labeled are grounded. The current through the quadruple dot array,  $I_{\text{array}}$ , is measured to create single dots. The reflectance of the SDs,  $V_{\text{RF,SD1}}$  and  $V_{\text{RF,SD2}}$  is monitored to tune DQDs into the single-electron regime. (b)–(d) Pinch-off curves showing  $I_{\text{array}}$  versus the gate voltages  $L$ ,  $P1$ , and  $D1$  ( $T = -400$  mV). The calculated transition value  $V_{\text{gate},i}^{\text{tr}}$  is shown as a dotted vertical line. The horizontal lines denote the high and low value of the current as detected by the algorithm.

composition of the heterostructure underneath each gate will be reflected in the required voltage to create quantum point contacts (QPCs). We term this voltage the transition value,  $V_{\text{gate},i}^{\text{tr}}$ , which is defined as the gate voltage for which  $I_{\text{array}}$  is at  $\sim 30\%$  of its maximum value (see supplementary material II A (Ref. 14)). This procedure is repeated for a range of  $T$ -values. Figs. 1(b)–1(d) show an example for  $T = -400$  mV and the gates controlling the leftmost dot ( $L$ ,  $P1$ , and  $D1$ ). In practice, it is best to continue with the most positive  $T$ -value that still allows pinch-off for all gates. In our experience, this tends to create better quantum dots for this gate design.

We start by creating single quantum dots, as they already include much of the cross-talk between gates, dots, and barriers, which are present in double dots. To create single quantum dots, we apply a fixed voltage for the plunger gate (usually  $-80$  mV) which we know is appropriate for this device design, and use the transition values of the barrier gates as input for a 2D coarse scan. A suitable scan range is  $[V_{\text{gate},i}^{\text{tr}} - 10$  mV,  $V_{\text{gate},i}^{\text{tr}} + 400$  mV]. We again monitor  $I_{\text{array}}$ . The structure of these scans is always similar: for negative gate voltages, the channel is closed, so there is no current. For more positive voltages, the channel is open, so there is a large current. We fit a tetragon to the area corresponding to large current, see Fig. 2(a) for an example of the leftmost dot (details can be found in the supplementary material II B (Ref. 14)). We next take a finer scan of the area closest to the tetragon corner with the most negative gate voltages; see Figs. 2(b)–2(e). In the experiments we have performed, this point is always showing the start of quantum dot formation through the appearance of a Coulomb peak. We use this point as the starting point in gate-space for creating DQDs. The exact location of the Coulomb peak is determined using a Gabor filter and is shown as black dots in Figs. 2(b)–2(e) (see supplementary material II B (Ref. 14)).

When going to double dots, transport measurements are not suitable as current levels through few-electron double dots are impractically low for this device design. Therefore, once the single dots have been formed, we tune the SDs in a similar way. They can then be used for non-invasive charge sensing which does allow one to distinguish single-electron

transitions in the dot array through RF-reflectometry. To achieve a high sensitivity, it is important that the SD is tuned to the flank of one of its Coulomb peaks. After finding a Coulomb peak for the SD in a similar way as described for the qubit dots, we make a 1D scan of the plunger gates; see Fig. 2(f). Each detected Coulomb peak is given a score based on its height and slope that allows the algorithm to continue with the most sensitive operating point for the corresponding plunger gate (see supplementary material II C (Ref. 14)).

With the SD tuned, we create a double dot in the following way: first, we set the voltages of the gates for the double dot to the values found for the individual single dots (black dots in Figs. 2(b)–2(e)). For the single gate shared by the two individual dots (e.g., gate  $D1$  for the leftmost double dot), the average of the two values is used. Next, we record a charge stability diagram of the double dot structure by varying the two plunger gate voltages involved. We use a heuristic formula to determine the correct scan range that takes into account the capacitive coupling of the gates to the dots (see supplementary material II D (Ref. 14)). Typical results for such scans are shown in Figs. 3(a)–3(c). Scans involving two plungers are measured by applying a triangular voltage ramp to the plungers on the horizontal axis using an arbitrary waveform generator, and by stepping the other plunger gate using DACs.<sup>15</sup> Whilst stepping the latter gate, we also adjust the sensing dot plunger gate to compensate for cross-capacitive coupling and thereby improve the operating range of the SD.

To verify that the double dot has reached the single-electron regime, the algorithm first detects how well specific parts of the charge stability diagrams match the shape of a reference cross (see inset of Fig. 3). Each match should ideally correspond to the crossing of a charging line from each dot. The shape of the reference cross is derived from the various capacitive couplings, which follow from the gate design and are known approximately from the start. Instead of detecting crosses, one could also try to detect the individual charge-transition lines. This turned out to be more sensitive to errors for two reasons: (1) Extra features in the charge stability diagrams that do not correspond to charging lines are wrongfully interpreted as dot features. (2) Not all

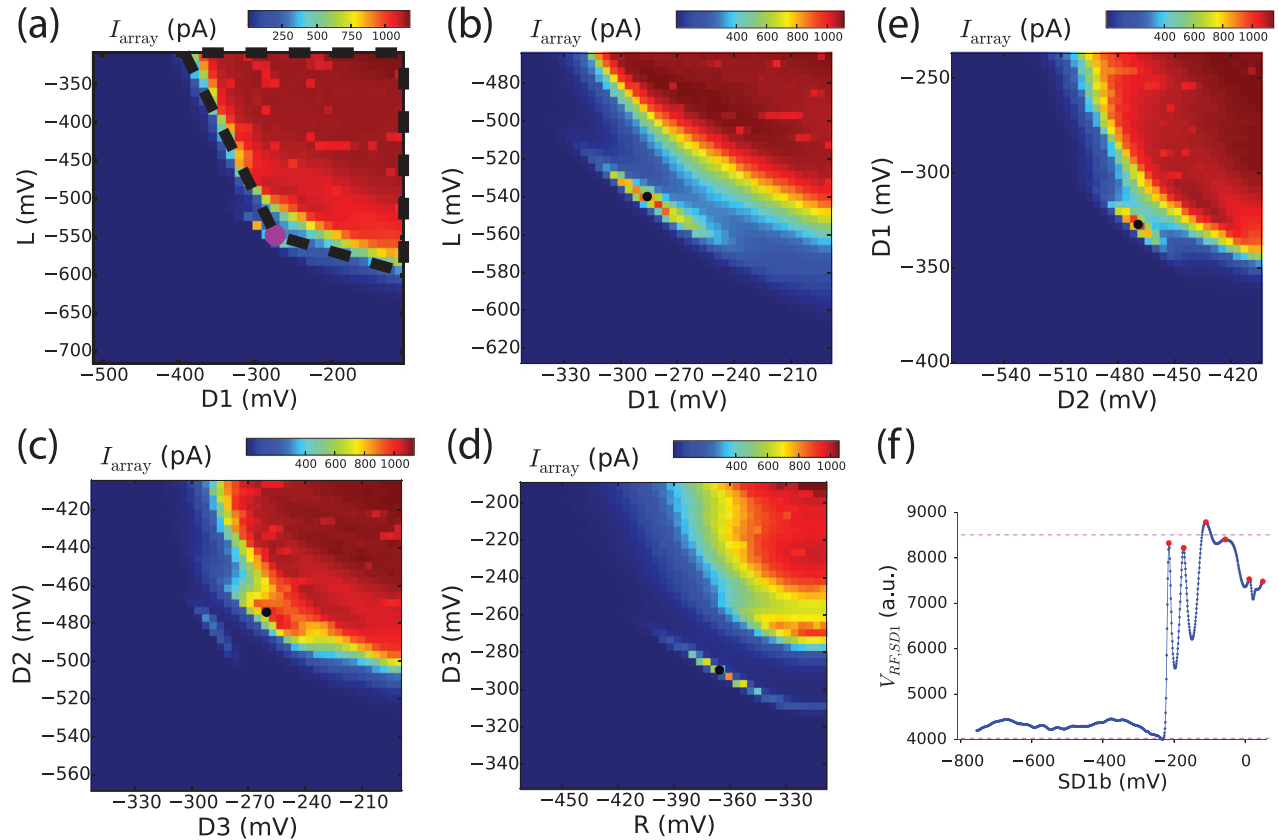


FIG. 2. (a)–(e) Four single dots are created by sweeping the tunnel barrier gate voltages for each dot whilst keeping the plunger gate fixed and monitoring  $I_{\text{array}}$ . After a coarse scan (example shown for the leftmost dot in (a)) we zoom in to the region showing Coulomb blockade (b)–(e). The center location where Coulomb peaks are formed is determined using a Gabor filter and depicted by black dots. (f) The SD is fine-tuned by sweeping its plunger gate voltage. The charge sensing measurements shown in Fig. 3 are performed by tuning to the left flank of a Coulomb peak.

charging lines are straight across the entire dataset; this makes it harder to interpret which line belongs to which dot. The cross-matching algorithm is robust against such anomalies because of the local, instead of global, search across the dataset. In future work, it could actually be useful to still

detect these extra and/or curved lines. They could give information about, e.g., unwanted additional dots and aid in determining the electron numbers in regions with higher tunnel couplings. For the current goal of finding the single-electron regime, this extra information is not required.

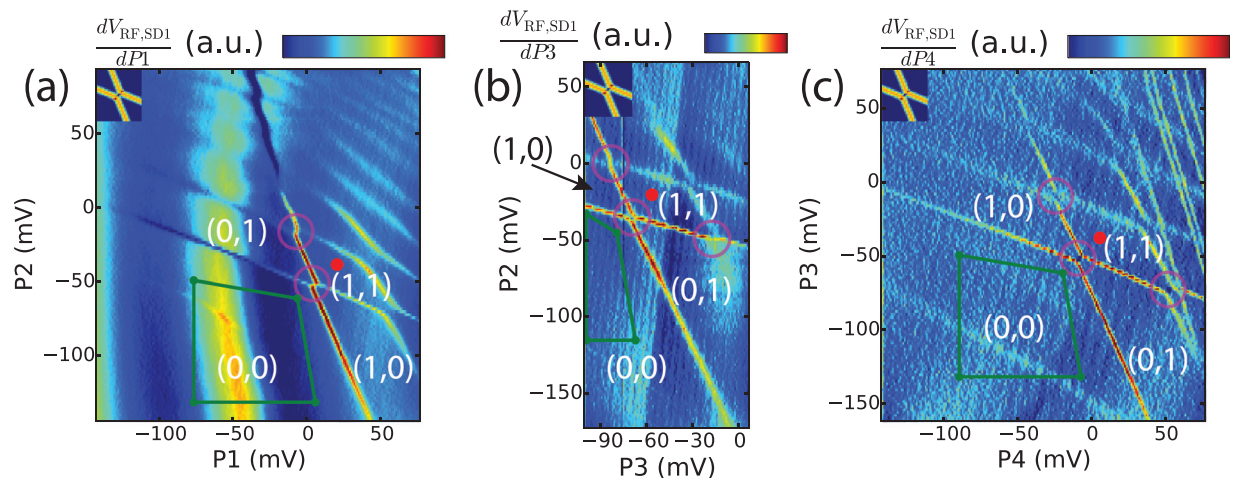


FIG. 3. (a)–(c) Double dot charge stability diagram for the left, middle and right double dot respectively. Using the result of Figs. 2(b)–2(e) the tunnel barriers are set, and the plunger gates are swept as indicated. The occupancy of each dot is denoted by  $(n, m)$  corresponding to the number of electrons in the left and right dot respectively of that specific double dot. The algorithm determines how well regions of the charge stability diagram match to a reference cross (see inset). Good matches are encircled. These are interpreted as crossings of charging lines from two dots. The single-electron regime is found by verifying that no other prominent charging lines are observed for more negative gate voltages with respect to the most bottom-left detected cross (green regions). The extra features present in (a) and (c) were below the detection threshold and are attributed to additional dots due to a lack of coupling with the double dot under investigation (a) or a different slope (c). These unwanted dots do not necessarily pose a problem for follow-up double dot experiments. The horizontal scan range of panel (b) is less than for (a) and (c) due to hardware limitations.



Next, the algorithm checks whether within a region slightly larger than  $70 \times 70 \text{ mV}^2$ , it finds other charge transitions for more negative gate voltages with respect to the most bottom-left detected cross. If this region is too small to draw a conclusion, the algorithm will adjust the scan range to more negative voltages (see supplementary material II D (Ref. 14)). The regions are depicted by the green tetragons in Fig. 3. If no extra transitions are detected: the single-electron regime has been found, and the result is given a score of 1 for that specific measurement outcome. If extra transitions are found, the algorithm outputs the score 0. For a score of 1, the algorithm can set both plunger voltages to  $+15 \text{ mV}$  with respect to the most bottom-left detected cross to enter the single-electron regime (depicted by red dots in Fig. 3). This is where the algorithm stops. At the end of the run the user can see the measurement results for the various initial choices of  $T$  and select the best one.

All combined, the running of this complete algorithm (for a single value of the  $T$ -gate) takes  $\sim 200 \text{ min}$  (see supplementary material II E (Ref. 14)). Per device typically  $5T$ -values are tested. In practice, we have observed that for some cool-downs of the sample the algorithm could not attain the single-electron regime. A thermal cycle combined with different bias cooling<sup>16</sup> can significantly influence the tuning and solve this issue; just as for tuning done by hand. The key difference is that with the computer-aided tuning, hardly any user effort is required to explore tuning of double dots to the few-electron regime. In future work, the time required for automated tuning (as well as for tuning by hand) can be further reduced by also connecting the tunnel barrier gates of each single dot to a high-frequency line which would allow much faster scans for Figs. 1 and 2.<sup>17</sup> These scans currently form the bottleneck in the overall tuning process. Future experiments will also address the automated tuning of more than two dots and the tuning of the tunnel couplings in between dots and their reservoirs, which are key parameters for operating dots as qubit devices. Finally, we expect that the same algorithm can be applied with minor modifications to a wide variety of gate-defined quantum dot devices, whether operating in depletion mode<sup>1,4,5,8,11,13,15</sup> or accumulation mode,<sup>9,10</sup> and whether they are based on 2D or 1D<sup>6,7,17</sup> electron systems. In particular, the main steps (identify pinch-off voltages, use those to create single dots, and use those as the starting point for double dots) apply in spirit across all such realizations. Furthermore, the Gabor filter and reference cross approaches for data interpretation can be adopted without modification.

In summary, we have demonstrated computer-automated tuning of double quantum dot devices into the

single-electron regime. This work will simplify tuning dots in the future and forms the first step towards automated tuning of large arrays of quantum dots.

The authors acknowledge useful discussions with the members of the Delft spin qubit team, and experimental assistance from M. Ammerlaan, J. Haanstra, R. Roeleveld, R. Schouten, M. Tiggelman, and R. Vermeulen. This work was supported by the Netherlands Organization of Scientific Research (NWO) Graduate Program, the Intelligence Advanced Research Projects Activity (IARPA) Multi-Qubit Coherent Operations (MQCO) Program, and the Swiss National Science Foundation.

- <sup>1</sup>R. Hanson, L. P. Kouwenhoven, J. R. Petta, S. Tarucha, and L. M. K. Vandersypen, *Rev. Mod. Phys.* **79**, 1217 (2007).
- <sup>2</sup>F. A. Zwanenburg, A. S. Dzurak, A. Morello, M. Y. Simmons, L. C. L. Hollenberg, G. Klimeck, S. Rogge, S. N. Coppersmith, and M. A. Eriksson, *Rev. Mod. Phys.* **85**, 961 (2013).
- <sup>3</sup>C. Kloeffel and D. Loss, *Annu. Rev. Condens. Matter Phys.* **4**, 51 (2013).
- <sup>4</sup>J. R. Petta, A. C. Johnson, J. M. Taylor, E. A. Laird, A. Yacoby, M. D. Lukin, C. M. Marcus, M. P. Hanson, and A. C. Gossard, *Science* **309**, 2180 (2005).
- <sup>5</sup>K. C. Nowack, F. H. Koppens, Y. V. Nazarov, and L. M. K. Vandersypen, *Science* **318**, 1430 (2007).
- <sup>6</sup>H. O. H. Churchill, A. J. Bestwick, J. W. Harlow, F. Kuemmeth, D. Marcos, C. H. Stwertka, S. K. Watson, and C. M. Marcus, *Nat. Phys.* **5**, 321 (2009).
- <sup>7</sup>Y.-Y. Liu, J. Stehlik, C. Eichler, M. J. Gullans, J. M. Taylor, and J. R. Petta, *Science* **347**, 285 (2015).
- <sup>8</sup>J. Medford, J. Beil, J. M. Taylor, S. D. Bartlett, A. C. Doherty, E. I. Rashba, D. P. Divincenzo, H. Lu, A. C. Gossard, and C. M. Marcus, *Nat. Nanotechnol.* **8**, 654 (2013).
- <sup>9</sup>E. Kawakami, P. Scarlino, D. R. Ward, F. R. Braakman, D. E. Savage, M. G. Lagally, M. Friesen, S. N. Coppersmith, M. A. Eriksson, and L. M. K. Vandersypen, *Nat. Nanotechnol.* **9**, 666 (2014).
- <sup>10</sup>M. Veldhorst, J. C. C. Hwang, C. H. Yang, A. W. Leenstra, B. de Ronde, J. P. Dehollain, J. T. Muhonen, F. E. Hudson, K. M. Itoh, A. Morello, and A. S. Dzurak, *Nat. Nanotechnol.* **9**, 981 (2014).
- <sup>11</sup>R. Thalneau, S. Hermelin, A. D. Wieck, C. Bäuerle, L. Saminadayar, and T. Meunier, *Appl. Phys. Lett.* **101**, 103102 (2012).
- <sup>12</sup>T. Takakura, A. Noiri, T. Obata, T. Otsuka, J. Yoneda, K. Yoshida, and S. Tarucha, *Appl. Phys. Lett.* **104**, 113109 (2014).
- <sup>13</sup>C. Barthel, M. Kjaergaard, J. Medford, M. Stopa, C. M. Marcus, M. P. Hanson, and A. C. Gossard, *Phys. Rev. B* **81**, 161308 (2010).
- <sup>14</sup>See supplementary material at <http://dx.doi.org/10.1063/1.4952624> for additional information on the used methods and materials, and details of the software and algorithms.
- <sup>15</sup>T. A. Baart, M. Shafiei, T. Fujita, C. Reichl, W. Wegscheider, and L. M. K. Vandersypen, *Nat. Nanotechnol.* **11**, 330 (2016).
- <sup>16</sup>A. R. Long, M. Pioro-Ladrière, J. H. Davies, A. S. Sachrajda, L. Gaudreau, P. Zawadzki, J. Lapointe, J. Gupta, Z. Wasilewski, and S. A. Studenikin, *Phys. E (Amsterdam, Neth.)* **34**, 553 (2006).
- <sup>17</sup>J. Stehlik, Y.-Y. Liu, C. M. Quintana, C. Eichler, T. R. Hartke, and J. R. Petta, *Phys. Rev. Appl.* **4**, 014018 (2015).